Q. J. R. Meteorol. Soc. (2002), **128**, pp. 893–912

Upstream influence of numerically simulated squall-line storms

By ROBERT G. FOVELL*
University of California, Los Angeles, USA

(Received 7 March 2001; revised 2 November 2001)

SUMMARY

The squall line's impact on its upstream environment is examined using traditional cloud and simplified (parametrized moisture) models. The study was motivated by the need to explain significant differences between the two dynamical frameworks. In both, the first environmental response to the convection consists of a rapidly propagating gravity wave characterized by deep tropospheric subsidence. This gravity wave accelerates the low-level storm inflow in its wake, with the largest effect seen near the surface.

In the more sophisticated model, however, this wave is eventually followed by a shorter vertical wavelength feature, one possessing lower-tropospheric ascent. This second gravity wave, absent from the simplified model runs, substantially alters the upstream environment yet again. The gentle low-level uplift establishes the 'cool/moist tongue' of air that has been found to stretch well ahead of the storm in simulations. Between the second wave and the main storm updraught, the accelerated inflow is shifted from the ground to the middle troposphere where it helps to push dry air into the convecting region.

This subsequent environmental adjustment responds to the establishment of a small yet persistent area of weak cooling during the early mature phase. Located in the middle troposphere at the upstream edge of the main cloud mass, this cooling is the combined effect of cloud-water evaporation and the ascent of subsaturated air. Though the cooling that excites it is of relatively small magnitude (<2 K), this wave's effect is dramatic and significant. A crude fix to the moisture parametrization served to establish a qualitatively similar tongue-like feature in the simplified model simulations, bringing the results from the two dynamical frameworks more into line.

KEYWORDS: Gravity waves Multicell storms Parametrized-moisture models

1. INTRODUCTION

Traditionally, cloud models have assumed horizontally homogeneous and temporally invariant base-state conditions and have initiated convection in relatively crude manners. The former simplifications can be advantageous for dynamical studies as any alterations which ensue in the storm's surrounding environment must be attributed to the storm (or model) itself. Despite this, traditional cloud models are still very nonlinear and complicated. Much of this is due to the model microphysics, including water substance phase changes, conversion rates, hydrometeor fallspeeds, etc.

Significant simplification could be realized by completely parametrizing moisture and its effects. However, the parametrized-moisture (PM) model's usefulness would be severely limited if it could not generate reasonably realistic circulations. Fovell and Tan (2000) (hereafter FT00) assessed the performance of a PM model formulation based on, and inspired by, Garner and Thorpe (1992) (hereafter GT). This PM model made latent-heat release conditionally proportional to ascent velocity and used a heat sink of specified size and intensity to generate and maintain the sub-cloud cold pool.

FT00 showed that the PM model can support realistic, sustained 'multicellular' behaviour in which storm longevity is assured by the sequential generation of short-lived convective cells. Multicell storms are ubiquitous in nature as well as among traditional cloud model simulations. The PM model's ability to capture this behaviour lent support to Fovell and Tan's (1998) (hereafter FT98) analysis of the sustained transience which minimized the role of microphysical details in causing the unsteadiness.

Less realistically, the PM model storms were found to exert a dramatic and permanent influence on the lower troposphere on their upstream sides, representing the

* Corresponding address: Department of Atmospheric Sciences, University of California, Los Angeles, Los Angeles, CA 90095-1565, USA. e-mail: rfovell@ucla.edu

environment into which the storms were propagating. The mature-phase low-level storm inflow was considerably intensified in the FT00 and GT simulations, with the largest enhancement found very near the ground. This occurred with both low and moderate convective available potential energy (CAPE) soundings, in multicellular as well as nearly steady cases. In the moderate CAPE case that FT00 highlighted, for example, the surface inflow changed by $\approx$10 m s^{-1} subsequent to convective initiation (see FT00 Fig. 7). In contrast, typical full-physics simulations evince little inflow enhancement in the lowest 2 or 3 km or so (Fovell and Ogura 1988) during maturity.

Certainly, the convection is expected to cause some upstream modification. A fraction of the storm updraught mass overturns to form the forward anvil, and mass continuity dictates some inflow enhancement must accompany that upper-tropospheric outflow. However, this influence seemed exaggerated and thus FT00 tried to isolate the apparent flaw in the PM framework. FT00 focused on mechanisms that might account for a PM model tendency to generate excessive anvil outflow strength. They suggested that excess warming in a mature PM storm's trailing region, a consequence of the PM model assumptions, might be the culprit.

In this paper, we examine more closely how and why the storm's upstream environment becomes disturbed by convection. Detailed intercomparisons of simulations made with the PM and full-physics models are made, with particular attention paid to how the mature storm structures come about. Further analysis of FT00's results revealed that the most significant difference between the two models resided in the *vertical structure*, rather than the magnitude, of the upstream disturbances. The root of this discrepancy is identified and confirmed via a practical 'fix' to the PM framework. However, the main intent of this study is to further elucidate the effect convection can exert on its immediate surroundings, and employment of two different model frameworks in juxtaposition serves this end.

2. Comparison of the traditional and parametrized-moisture cloud models

In this section, the environmental responses to convective heating in the PM and traditional models are described and compared. The storms in this paper propagate towards the east, and the terms 'downstream' and 'upstream' are synonymous with 'west' and 'east', respectively. The upstream side is also downshear relative to the initial vertical shear vector. The horizontal velocity field u will be presented in domain-relative (u_{dom}) and ground-relative (u_{grnd}) perspectives and will also be expressed as a perturbation from the initial state (u'). The domain is translated and thus u_{dom} usually closely approximates storm-relative velocity (u_{strm}). The perturbation field is independent of the reference frame. The ground-relative initial wind is taken to be calm at the model surface.

(*a*) *A parametrized-moisture model simulation*

The PM framework (see Fig. 1) was described in detail in FT00. Briefly, the chief effects of moisture are parametrized through the inclusion of terms representing vapour-condensation warming and liquid-water evaporation, labelled Q^+ and Q^-, respectively. These terms appear in the model's perturbation potential temperature (θ') equation as

$$\frac{\mathrm{d}\theta'}{\mathrm{d}t} = Q^+ + Q^-. \tag{1}$$

This perturbation is relative to a base state which is a function of height alone.

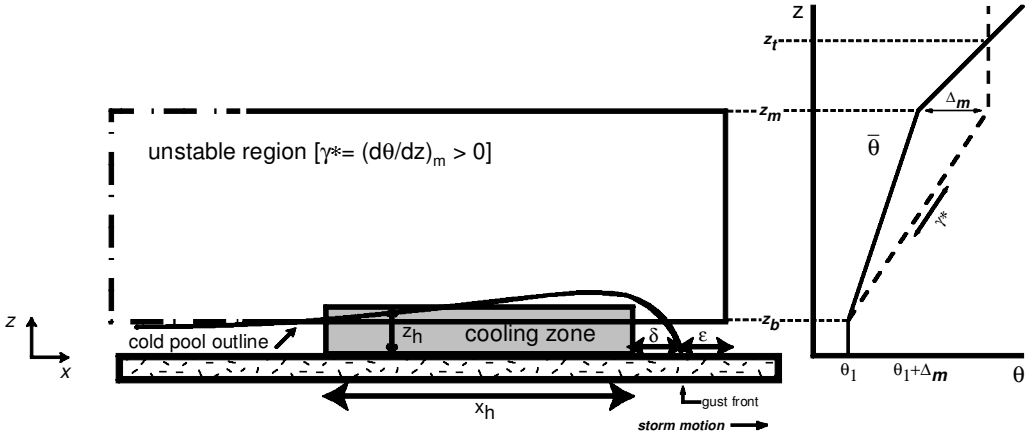

Figure 1. Schematic illustrating the parametrized-moisture model implementation. Fovell and Tan's (2000) low convective available potential energy (CAPE) sounding is depicted on the right. Values of 1, 7 and 9 km for z_b, z_m and z_t, respectively, along with $\Delta_m = 3$ K were used for this sounding. See text for further explanation.

The evaporation cooling term Q^- is treated as a shallow, lower-tropospheric cooling zone of dimensions $x_h \times z_h$, in which air is continuously relaxed to the preset potential-temperature perturbation θ'_c with a designated time-scale τ_c. The sink's upstream edge is positioned a small distance δ behind the storm's gust front, subsequent to that feature becoming established. As per usual, model domain translation attempts to keep the gust front as stationary as possible, but domain-relative motion can still occur in some cases. The cooling zone's alignment relative to the front is examined every time step, and shifted if necessary to keep the two properly oriented.

In the PM model latent-heat release is made proportional to ascent velocity ($w > 0$) by presuming air rises moist adiabatically within the 'cloud'. Designating the slope of the moist adiabat in (θ, z) space as γ^*, Q^+ is handled as

$$Q^+ = \gamma^* \max(w, w_0) \tag{2}$$

where heretofore $w_0 = 0$. The 'unstable region', the sub-domain in which γ^* is non-zero, resides between height levels z_m and z_b (Fig. 1); level z_t merely serves to define the model stratospheric stability. Further, the region stretches laterally rearward to the domain's downstream boundary but its upstream extent is truncated a small distance ϵ ahead of the surface gust front's position. FT00 reported this truncation had virtually no effect on their simulations; we explain this result presently. As in FT00, both δ and ϵ are taken to be 5 km.

Figures 2 and 3 present typical multicellular PM model simulations, emphasizing the organizational period during which the environmental alteration develops. These examples employed FT00's low- and moderate-instability soundings, having 400 and 1800 J kg^{-1} of CAPE, respectively (see Fig. 1 and FT00's Fig. 4). Note that the ambient stability of the low-CAPE sounding is also quite small; the moderate-CAPE case, based on FT98's initial environment, possesses a realistic background state.

Middle-tropospheric warming, manifested as positive potential-temperature perturbations (θ'), is seen spreading outward from the centre of convective activity in both simulations. The induced horizontal-velocity perturbations (u') are directed away from (towards) the convective region above (below) the level of maximum warming. On the upstream (east) side of each case, the largest outflow is located at the level at which

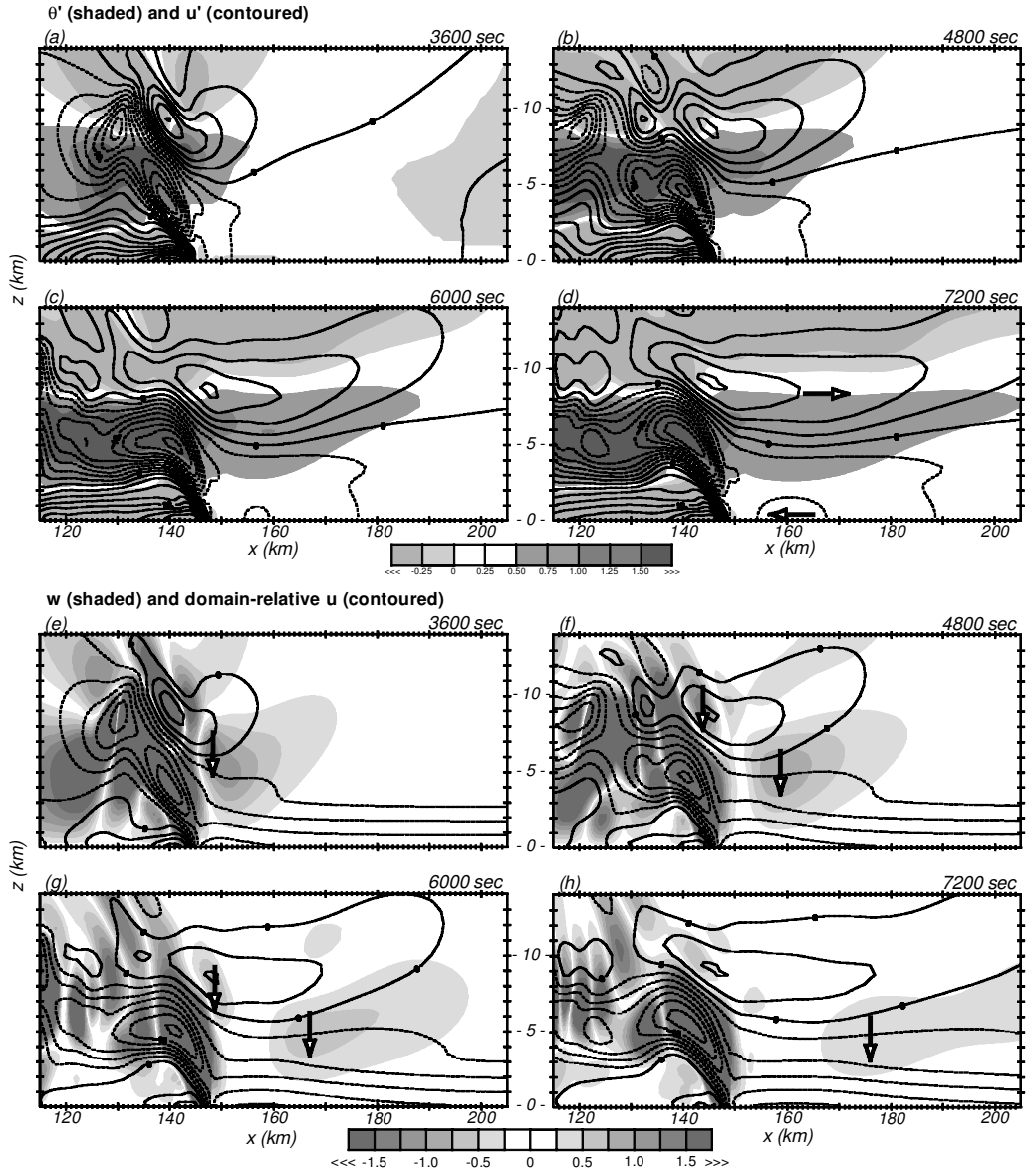

Figure 2. Low convective available potential energy (CAPE) parametrized-moisture model simulation, having moderate low-level shear of 3.15×10^{-3} s^{-1} below 3 km. (a)–(d) show perturbation horizontal velocity (u', 2 m s^{-1} contours) and perturbation potential temperature (θ', shaded); (e)–(h) present domain-relative horizontal velocity (u_{dom}, 3 m s^{-1} contours) and vertical velocity (w, shaded). Only a portion of the model domain is shown, and horizontal distance is measured from the west edge of the fine-grid region; see Fovell and Tan (2000). Domain was translated eastward at 11.5 m s^{-1}.

the temperature perturbations vanish (about 9–10 km). Note that the strongest inflow is located just above the model's free-slip bottom surface.

The vertical velocity (w) fields in Figs. 2 and 3 reveal that the leading edge of the environmental adjustment, GT's 'storm-front', is marked by deep subsidence. Focusing on the upstream environment, the subsidence is seen to propagate eastward away from the convection, leaving in its wake a permanently altered flow field. Note the dashed

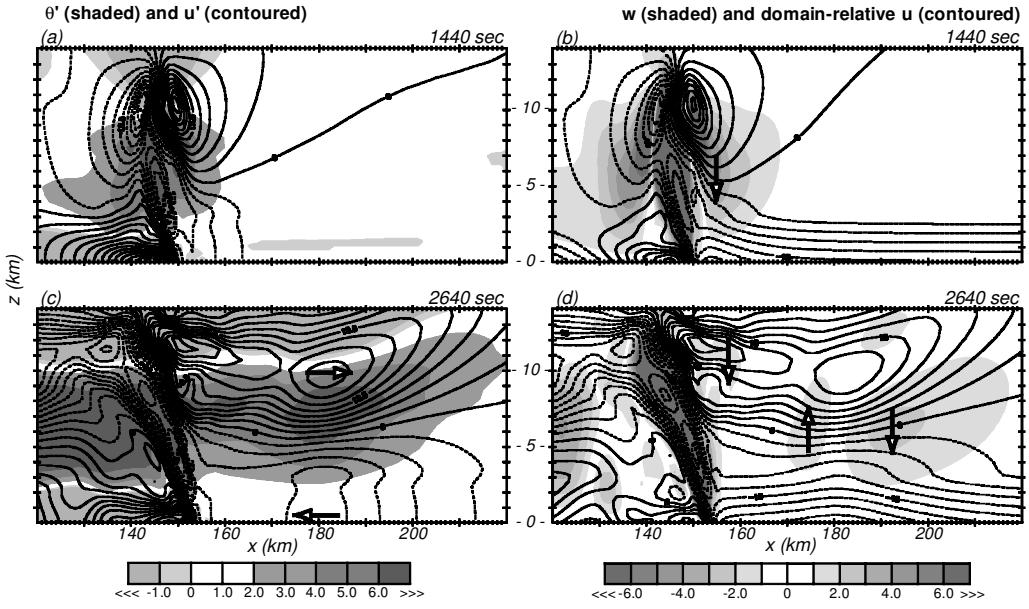

Figure 3. As in Fig. 2 but for a moderate convective available potential energy (CAPE) parametrized-moisture model simulation having 5×10^{-3} s^{-1} of shear below 3 km. (a) and (c) show u' (2.5 m s^{-1} contours) and θ' (shaded); (b) and (d) present u_{dom} (3 m s^{-1} contours) and w (shaded). Only a portion of the model domain is shown. Domain was translated eastward at 15.4 m s^{-1}.

contours of domain-relative horizontal velocity (u_{dom}) are 'lifted' by the disturbance's passage, never to settle back to their original positions. In between the convection and the storm front, transience quickly disappears. While the environmental response is quicker to develop, has larger amplitude and faster propagation in the moderate-CAPE/realistic-stability case, there is substantial qualitative resemblance between the two environments.

Figure 4 presents a vertical profile of the ground-relative wind (u_{grnd}) taken 10 km ahead of the surface gust-front position for the low-CAPE case, along with the initial profile. Note that easterly perturbations, representing enhanced storm inflow, are present below 5 km, with the largest values at the ground. This profile was taken at $t = 10800$ s; the simulation had become statistically steady by this time, at least in the vicinity of the convection (and behind the spreading storm front). The moderate-CAPE run will be examined further in section 4.

(*b*) *A traditional cloud model simulation*

Now we turn to a rather typical multicellular simulation made with a traditional cloud model, specifically the Advanced Regional Prediction System (ARPS) model (Xue *et al.* 2000). The simulation, being FT98's two-dimensional (2D) case, started with a moderate CAPE ($\approx$2500 J kg^{-1}) environment with a vertical shear of 3×10^{-3} s^{-1} in a 2.5 km deep layer. Thus, the initial ground-relative flow above the shear layer was 7.5 m s^{-1}. The domain speed was 12 m s^{-1} during the time period depicted. Please refer to FT98 for additional information.

At first, the environment's response to the convection is rather similar to that seen in the PM model. Figure 5 presents w and u_{dom} fields sampling the early portion of

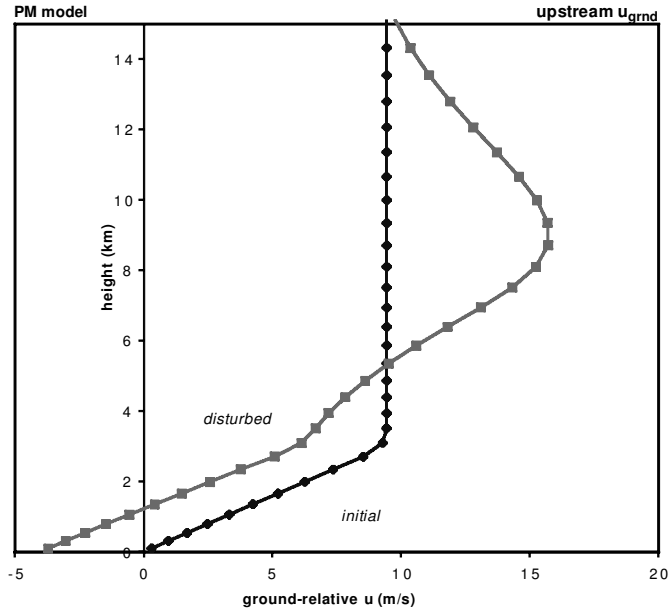

Figure 4. Vertical profile of ground-relative horizontal velocity (u_{grnd}) taken 10 km ahead of the surface gust-front position during the parametrized-moisture (PM) model storm's mature phase, compared with initial wind profile.

the model storm's organizational period. As in the PM model simulation, the initiation of convection provokes rapidly spreading subsidence waves. In this case, the upstream-propagating feature's domain-relative motion was about 33 m s^{-1}, making for a 45 m s^{-1} ground-relative signal*. The ground-relative speed for the downstream side's wave was about 30 m s^{-1}. As shown in Fig. 6, which presents θ' and u' fields for these same three times, the subsidence waves are again marked by warming. In the upstream-propagating feature's wake are westerly and easterly horizontal-wind perturbations, present above and below the location of maximum warming, respectively.

The principal difference between the PM and traditional model simulations at this point concerns transience in the model storm upstream environment. The full-physics storm's main updraught underwent dramatic fluctuations between vertical and downshear (upstream) tilted orientations, exciting a sequence of similar, semi-discrete wave-like features (see especially Fig. 5(c)) which propagated through the upstream environment. This was possibly suppressed in the PM model by the nature of the moisture parametrization. The main point is that the ground-relative perturbations at this time are easterly and westerly in the lower and upper troposphere, respectively, with the largest inflow enhancements found very near the surface.

Figure 7 shows θ' and u' fields for the period 3900–4500 s. By 3900 s (Fig. 7(a)), the sub-cloud cold pool was well formed and the storm's rising front-to-rear airflow had already acquired the characteristic upshear (downstream) tilt superposed with multicellular transience it would retain for the balance of the simulation. This figure roughly spans one cell generation period and focuses more narrowly on the storm's leading edge. The deep waves generated earlier have already moved upstream out of the

* This was not the fastest moving signal in this early period; much faster (but also much smaller amplitude) features are evident in u_{dom} contours' kinks.

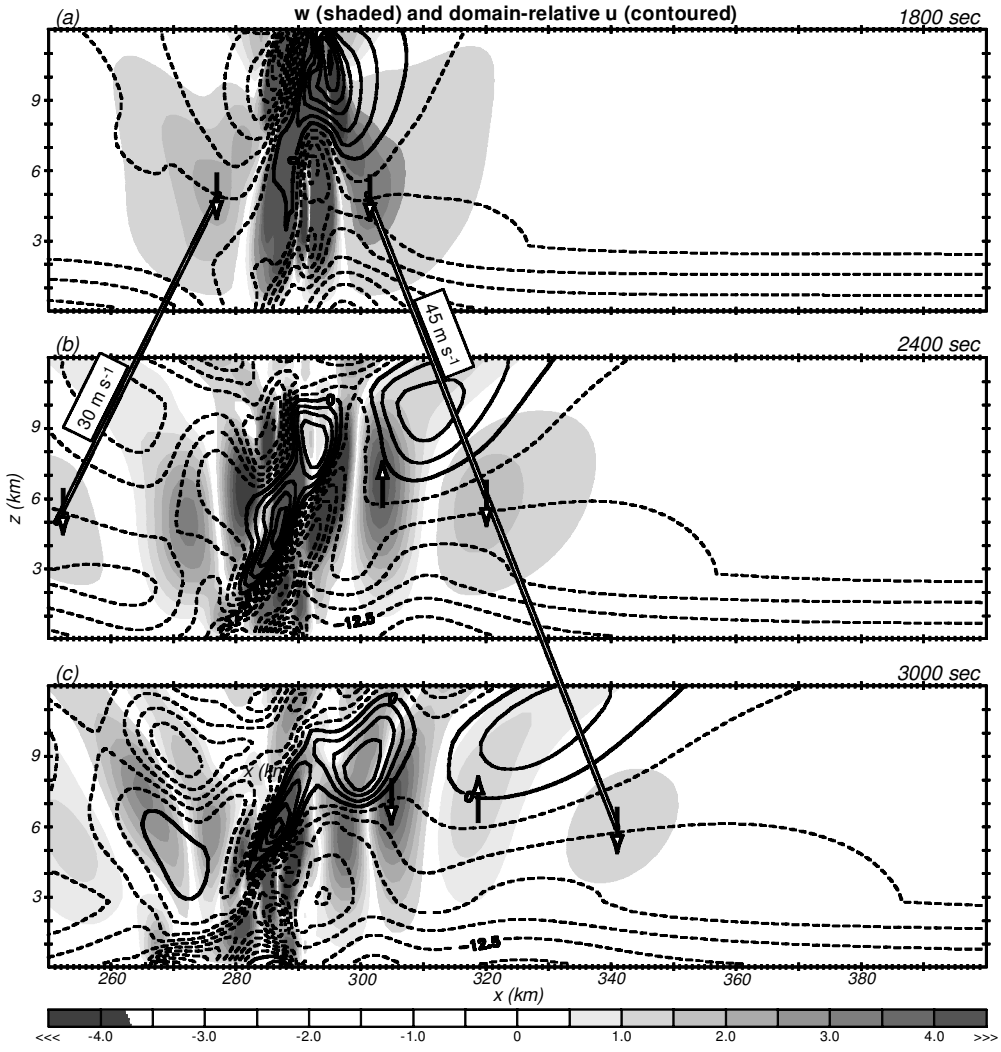

Figure 5. Early organizational period of the full-physics model simulation. Shown are the domain-relative horizontal velocity (u_{dom}, 2.5 m s^{-1} contours) and vertical velocity (w, shaded) for a portion of the model domain. Upstream and downstream movement of the initial subsidence wave is tracked and labelled with ground-relative propagation speed. Horizontal distance is measured from the west boundary.

sub-domain depicted although warming and westerly u' perturbations still occupy much of the upper troposphere. Large easterly perturbations are still present upstream of the convection but, importantly, *the level of maximum inflow enhancement has shifted to the middle troposphere* ($z \approx 5$ km). The near-surface perturbations just ahead of the storm are now rather small.

Note also the presence in all three panels of a tongue-like feature representing a small but sustained amount of mid-tropospheric cooling stretching across the storm's leading edge ($284 \leq \times \leq 292$ km). This feature will be designated the *cool/moist tongue* since it will presently be shown that its air has also been moistened relative to the initial state. Both the local cooling and nearby enhanced inflow are disturbed as the cell passes through its life cycle but appear to change in unison. The maximum inflow perturbation

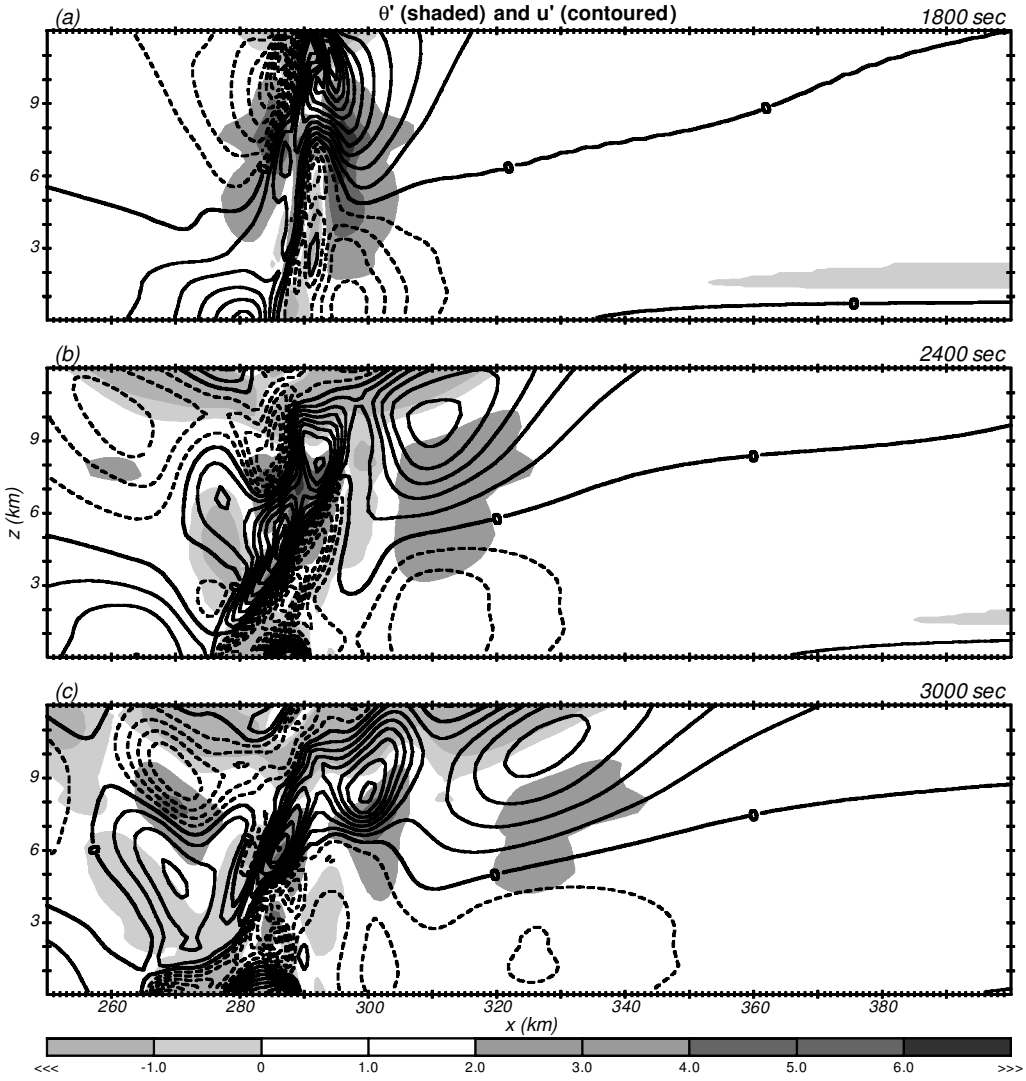

Figure 6. As in Fig. 5, but showing perturbation horizontal velocity (u', 2 m s^{-1} contours) and perturbation potential temperature (θ').

remains rooted just above this tongue. Though not shown, the cool/moist tongue also occurs in less geometrically constricted three-dimensional (3D) simulations as well.

Figure 8 provides a close-up view of the storm's leading edge, at a time one minute prior to that of Fig. 7(b). The θ' and w fields (Fig. 8(a)) show the cool/moist tongue forming a 'cap' hugging the top of the developing cloud and its updraught. This air has been moistened as well: Fig. 8(b) reveals positive water-vapour perturbation (q'_v) values throughout the tongue area.

The bottom two panels, along with Fig. 8(b)'s equivalent potential-temperature (θ_e) distribution, suggest that subsaturated air has been rising in the vicinity of the developing cloud and has been chilled by both adiabatic expansion and cloud-water evaporation. The latter, along with the general uplift, accounts for the moistening. Figure 8(c) shows

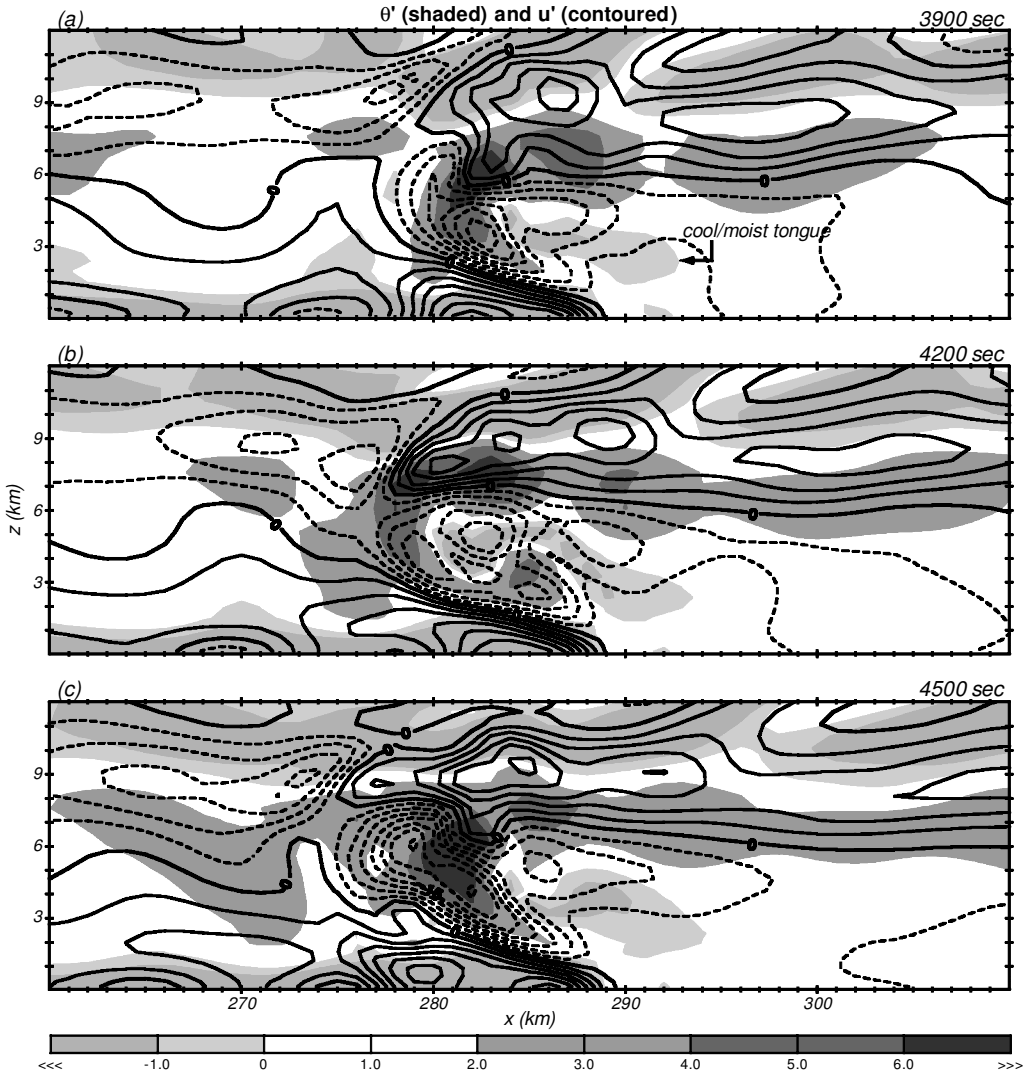

Figure 7. As in Fig. 5 but for a period straddling the organizational and mature phases.

the combination of the vertical potential-temperature advection (VPTA), expressed as

$$\mathrm{VPTA} = -w\frac{\partial\theta}{\partial z}, \tag{3}$$

and the cloud-water diabatic term, $S(q_c)$, for this instant in time*. The net effect of vertical advection and cloud-vapour phase changes is cooling through the tongue area. In Fig. 8(d) the $S(q_c)$ field is shown in isolation. Mixing of subsaturated air into the cloud continues to erode the cloudy area, resulting in part of the cooling seen.

* This combination comprises most of what FT98 termed 'TVPT' (see their Fig. 9), except for rainwater evaporation which is excluded here to highlight the cloud-water evaporation contribution. There is no rainwater for $x > 281$ km anyway.

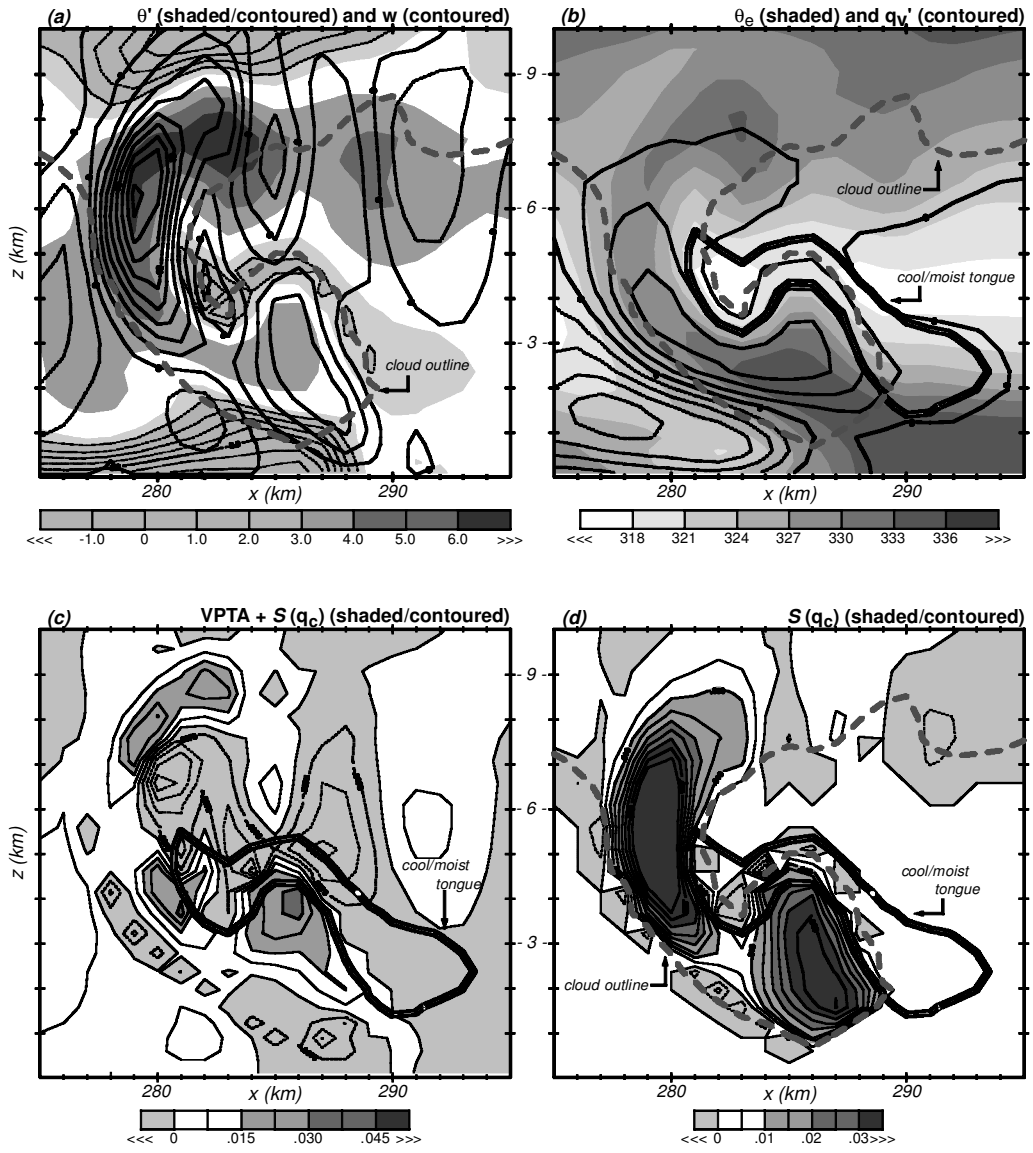

Figure 8. Close-up view of the storm's leading edge at 4140 s. (a) Vertical velocity (w, 2 m s^{-1} contours) and perturbation potential temperature (θ', shaded); (b) perturbation water-vapour mixing ratio (q'_v, 1 g kg^{-1} contours) and equivalent potential temperature (θ_e, shaded); (c) vertical potential-temperatur e advection (VPTA) and cloud-water diabatic heating/cooling ($S(q_c)$) combination (0.0075 K s^{-1} contours); (d) $S(q_c)$ (0.005 K s^{-1} contours). Cloud outline (0.1 g kg^{-1} mixing ratio) shown as grey broken curve is shown on panels (a), (b) and (d). Cool/moist tongue superposed on panels (b)–(d). Thin contours superposed on shaded fields in panels (a)–(c) highlight negative values.

The mid-tropospheric cooling continues to spread horizontally in the upstream direction over the next several hours. The times shown in Fig. 9 were chosen to represent roughly the same point within the multicellular repeat cycle. The leading edge of the cool/moist tongue is marked by a weak, propagating updraught (see Fig. 9(a)). The enhanced mid-tropospheric inflow also spreads, in lock step with the cooling; the correlation between these features will be explored in the next section. As these features

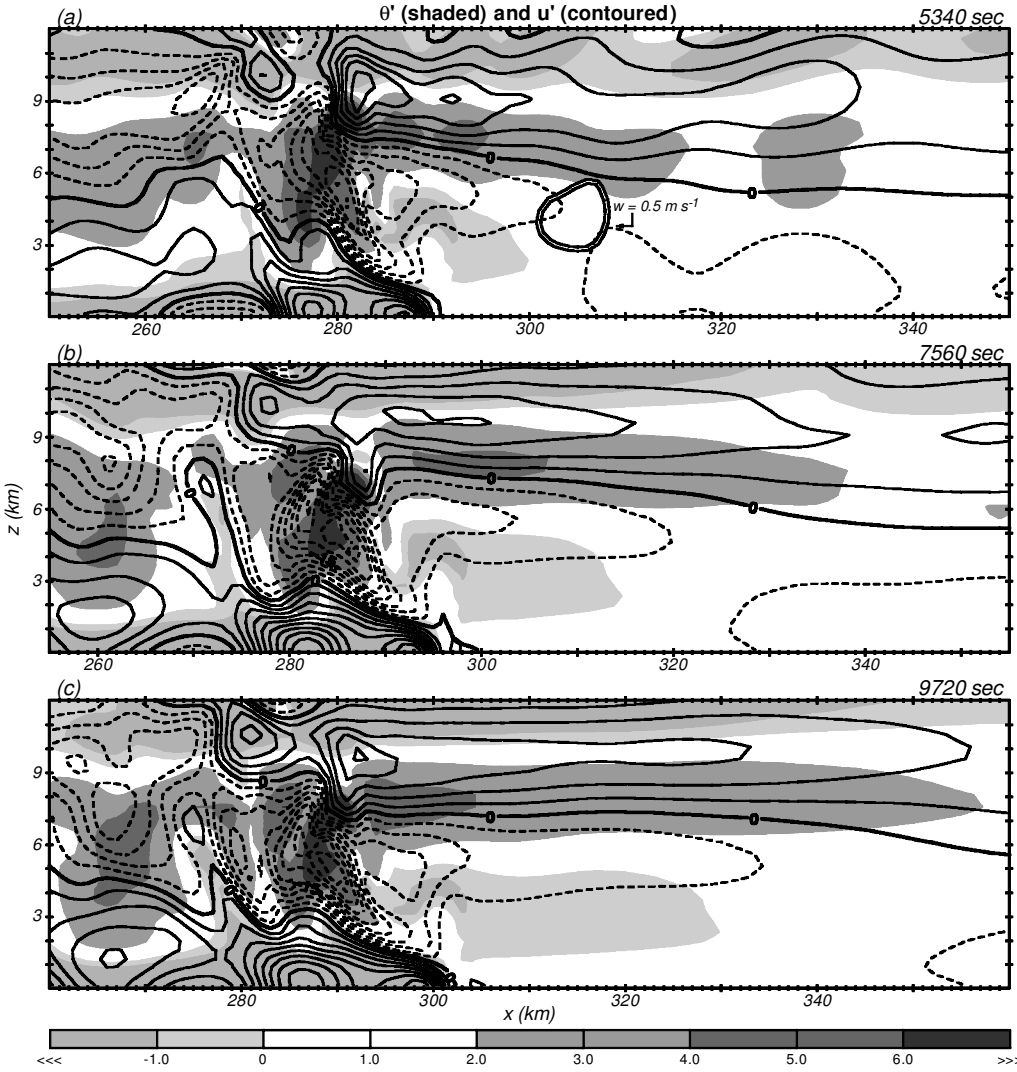

Figure 9. As in Fig. 7, but extending through the early mature phase.

widen, the upstream environment in the immediate vicinity of the convection settles into an essentially statistically steady mature state.

The vertical profile of u_{grnd} characterizing the upstream environment during this mature phase is shown in Fig. 10. In pointed contrast to the PM model results, the easterly wind perturbations are centred around 5 km, and only a very minor alteration to the storm's immediate low-level inflow can be noted. A very similar profile was found in Fovell and Ogura's (1988) (Fig. 13) moderate-intensity squall line; elevated upstream inflow also appears in the midlatitude cases simulated by Schmidt and Cotton (1990) (Fig. 11) and Nachamkin and Cotton (2000) (Fig. 10) as well as in Lafore and Moncrieff's (1989) (Fig. 4) tropical setting. A similar upstream response is even noted in very strong, nearly erect storms such as Fovell and Ogura's (1989) most highly sheared

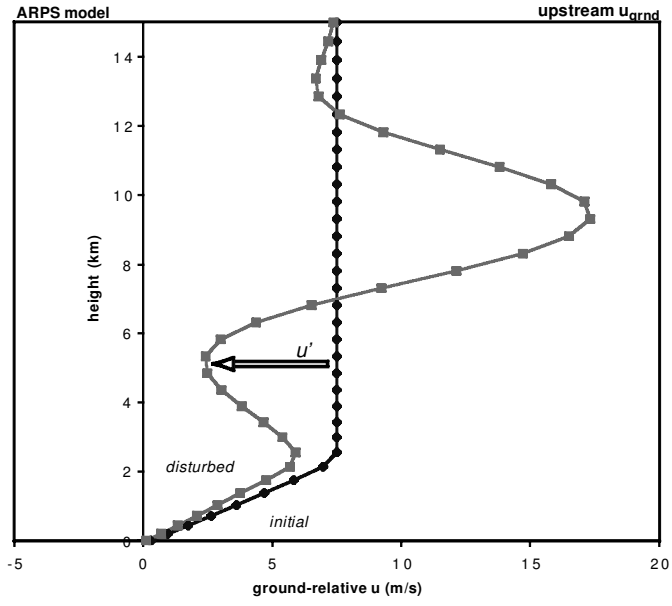

Figure 10. Vertical profile of the horizontal velocity relative to the ground (u_{grnd}) taken 10 km ahead of the surface gust-front position during the full-physics model (Advanced Regional Prediction System, ARPS) storm's mature phase and the initial wind profile, for comparison with Fig. 4.

cases (not shown); FT98's 3D storm during maturity was also strongly similar (also not shown).

3. Interpretation of these results

(*a*) *Results from analytic investigations*

Nicholls *et al.* (1991) (hereafter NPC) investigated the environmental response to maintained heat sources in an idealized setting. Their examination extended previous studies by Lin and Smith (1986) and Bretherton and Smolarkiewicz (1989), among others, and was itself further amplified by Mapes (1993). Using analytical solutions of the 2D linearized and hydrostatic Boussinesq equations, NPC demonstrated that a vertically oriented source immediately provokes subsidence of depth comparable to the source which then rapidly propagates away. This feature, clearly GT's storm front, is considered a gravity wave. It may be followed by a sequence of successively slower moving gravity waves which in combination constitute the aggregate environmental adjustment to convection.

The top two panels of Fig. 11 qualitatively depict the adjustment of an initially quiescent environment to a symmetric and vertically oriented heat source, based on information presented in NPC Figs. 3 and 5, and Mapes' Fig. 3. When the heating function possessed a single vertical mode (Fig. 11(a)), being a half-sine profile of depth H, this subsidence wave was the sole disturbance excited in the surrounding environment (at least in their analytic, linear and rigidly capped solution). This response had a vertical wavelength L_z of $2H$ and its intrinsic phase speed was well approximated by

$$c = \frac{NL_z}{2\pi}, \tag{4}$$

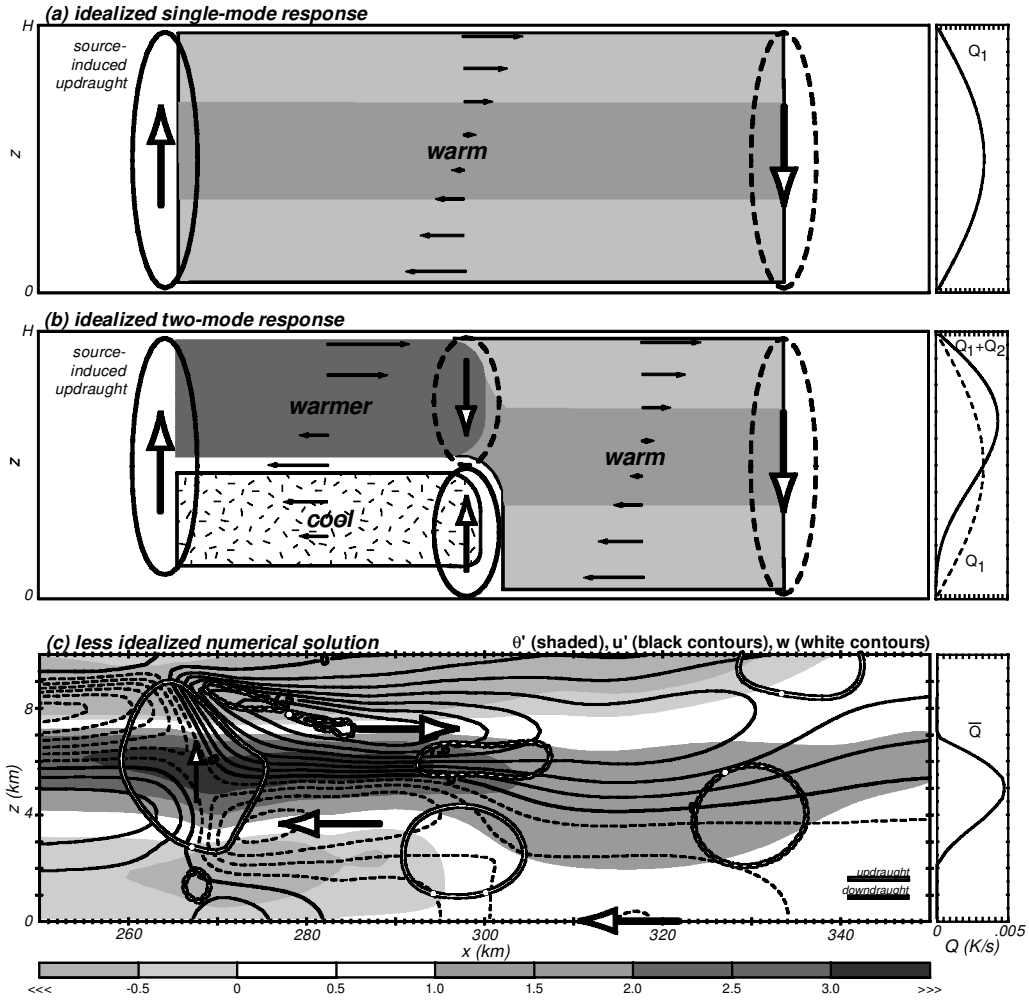

Figure 11. Environmental response to maintained heat sources. Top two panels qualitatively depict response to symmetric heating functions with (a) one and (b) two vertical modes, drawn from Nicholls *et al.* (1991) and Mapes (1993); only upstream side is drawn. Panel (c) presents numerical result for a less idealized situation. Heating functions shown on the right; for (c) the function is spatially averaged over the vertically tilted source region and has units of K s^{-1}.

where N is the tropospheric Brunt–Väisälä frequency. As this feature progressed away from the source, upper-tropospheric outflow (inflow) in the upper (lower) troposphere remained in its positively buoyant wake stretching between the storm front and the heat source. The largest enhanced flow towards the source was at the surface.

When other vertical modes were incorporated into this heating profile, additional environmental responses were excited. Specifically, a second vertical mode having heating and cooling each of depth $H/2$ was found to provoke a wave-like response having half the vertical wavelength and phase speed of the initial wave, the latter being given by Eq. (4). Thus, this second feature propagated through the wake of the initial subsidence wave, modifying its predecessor's environmental adjustment. NPC arranged their second mode to augment the upper-tropospheric heating of the first mode while introducing diabatic cooling into the lower troposphere. Mapes (1993) showed that

a qualitatively similar response could be obtained using source profiles having only positive values. In this scenario (depicted in Fig. 11(b)) the lower-tropospheric cooling still occurs, but it originates from *adiabatic expansion cooling* locally exceeding the applied heating.

However provoked, the shorter-wavelength feature possessed ascent confined to the lower troposphere. In its own wake, the previously established upper-tropospheric outflow became stronger and more concentrated. More importantly, *the enhanced inflow was shifted up to the middle troposphere*. As shown in Fig. 11(b), the strongest inflow was located where $\theta' = 0$, at the top of the adiabatically cooled layer.

These schematics were based on linear analytic solutions made using a vertically oriented heat source in a calm, constant N environment and a rigidly topped domain. Figure 11(c) presents a nonlinear numerical solution for a somewhat more realistic situation, made using a nonlinear and non-hydrostatic model. The initial conditions come from FT98, so the atmosphere is sheared as well as multiply layered, with an appreciably deep stratosphere. The heat source was tilted towards the west with height, mimicking the orientation of the storm's characteristic front-to-rear flow. The heating function itself represented a compromise between FT00's low- and high-CAPE environments. Perturbations from the initial horizontal wind field (i.e. u') are shown.

Even with these complications, the essential tropospheric response remains unchanged. It is noted that the addition of a cold pool for $x < 270$ km, with maximum cooling at the ground, could have eliminated the shallow layer of source-relative outflow that developed in the lower troposphere just ahead of the main updraught. This would have made the solution shown even more realistic with respect to the lower-tropospheric upstream response, an expectation consistent with Pandya and Durran's (1996) Fig. 20.

(*b*) *Application to the traditional cloud model simulation*

Figure 12 presents a Hovmöller diagram of Δu, defined here as the difference between u' values at the 5.4 and 0.1 km height levels, for the FT98 ARPS simulation. The 5.4 km level was chosen not only because it roughly corresponds to the height at which $u' = 0$ immediately following the initiation of convection (see Fig. 7) but also because it is the level at which the u' inflow maximum subsequently occurs. Thus, a positive Δu occurs when the induced inflow maximum is close to the ground, and negative values are obtained with elevated inflow. The reference frame is translating eastward at 12 m s^{-1}. During maturity, the model storm propagation speed is 15 m s^{-1} (3 m s^{-1}) relative to the ground (domain). All speeds labelled on the figure are ground relative.

The deep subsidence waves, the environment's first sizeable reaction to the convection, are seen to spread quickly in both directions away from the initial disturbance. Again (see Fig. 5), the ground-relative propagation speeds were 45 and 30 m s^{-1} for the eastward and westward moving features, respectively, values which correspond to an intrinsic phase speed of 37.5 m s^{-1}. (Above the 2.5 km deep shear layer, initial u_{grnd} is 7.5 m s^{-1}.) Referring to Eq. (4), this intrinsic speed is consistent with a gravity wave having a vertical wavelength of roughly twice the tropospheric depth H of 12 km*. During this period, the storm updraught is powerful and extends vertically through nearly the entire troposphere.

* Incidentally, the dependence in Eq. (4) on N explains why the signal propagated much more slowly in FT00's low-CAPE, low-stability sounding.

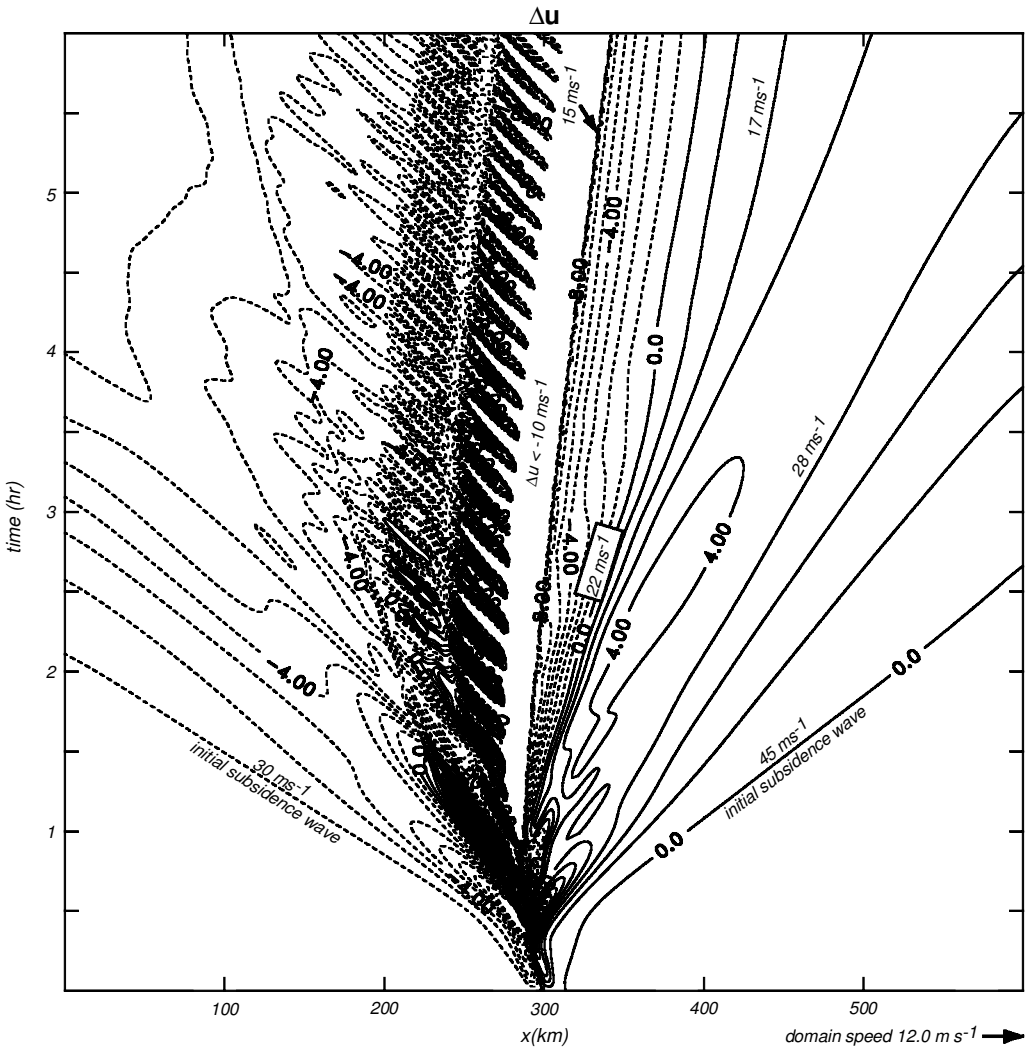

Figure 12. Hovmöller diagram depicting difference between horizontal-wind perturbations at 5.4 and 0.1 km (Δu, 1 m s^{-1} contours) for the full-physics simulation, presented in a domain-relative reference frame with ground-relative phase speeds superposed. Only $\Delta u > -10$ m s^{-1} values are shown.

The Δu values between the initial upstream wave and the convection are positive, reflecting the fact that the inflow enhancement is located in the lower troposphere. Progressively slower moving features, representing waves having shallower vertical structures, spread out in this original wave's wake. After an hour, negative Δu values appear in the vicinity of the convection and subsequently spread eastward. This represents the permanent shift of the enhanced inflow to the middle troposphere.

Based on the foregoing, we interpret this second feature as representing the environment's response to the essentially permanent adiabatic cooling that appears on the convective updraught's upstream side (as seen in Figs. 7 and 9). The ground-relative phase speed of this wave's leading edge is about 22 m s^{-1}. While the presence of the lower-tropospheric shear layer is probably a complicating factor in this case, it is

reasonable to presume this value represents an intrinsic phase speed of $\approx$16 m s^{-1}, corresponding to a source with a vertical half wavelength of about 5 km, about the depth over which the adiabatic cooling extends in the vicinity of the storm updraught. Behind this second principal feature, which slows somewhat as it spreads outward, the upstream environment settles into a statistically steady state.

The upstream propagation of this wave's updraught spreads the mid-tropospheric cooling upstream and moistens the lower troposphere. The presence of a cooled, moistened lower-tropospheric layer extending well upstream of the storm during maturity has been noted in squall-line simulations in the past (e.g. Fig. 11 of Fovell and Ogura (1988), Lafore and Moncrieff's (1989) Fig. 21(a) and FT98's Fig. 15). Observations may be more scarce, but at least Hoxit *et al.*'s (1976) analysis of a Nebraska squall line evinced a clear pre-squall elevated moist cool/moist tongue (their Fig. 4). FT98 remarked on the role of the elevated moisture in the triggering of new convective cells. The 'daughter clouds' they identified in the storm's immediate upstream environment resided in air brought to saturation by cooling and moistening within the tongue.

4. Evaluation and revision of the parametrized-moisture framework

In effect, the upstream environment in the more sophisticated model experiences two separate, successive adjustments to the establishment of convection, the first in response to the initial burst of deep tropospheric heating, and the second occurring once the principal storm updraught starts canting upshear. The PM model storms also tilt upshear, so it is not the tilt itself that is crucial. Rather, the subsequent adjustment proceeds once small yet sustained mid-tropospheric cooling appears in the vicinity of the convection, on the upstream side of the principal storm updraught. Like the first, the subsequent adjustment substantially and permanently modifies the upstream environment, this time effectively displacing the enhanced storm inflow to the middle troposphere.

This second adjustment is heretofore missing in the PM model owing to its inability to establish the localized cooling. In the PM model, all rising motion within the unstable region is presumed to be saturated, thus generating local warming, independent of the origin of the parcels being displaced. Thus, as presently formulated, the PM model is unable to detect which parcels are likely candidates for saturation and warming generation upon ascent, and which are not. Moreover, there is not any real cloud water to evaporate.

We have modified the moisture parametrization so that it roughly captures this small but crucial localized cooling. In so doing, we exploit our ability to control this cooling's presence in the PM model, thereby further supporting our analysis. Since the cooling typically appears on the periphery of the cell updraughts where vertical velocities are upward though small (Fig. 8), revising w_0, the threshold vertical velocity for triggering parametrized warming in Eq. (2), to be a small positive number (rather than exactly zero) seems to represent the simplest and most straightforward solution. This is an attempt to crudely mimic both adiabatic cooling of rising subsaturated air as well as the evaporation cooling owing to cloud water detrained into that air.

Figure 13 demonstrates the modification's influence when FT00's moderate-CAPE environment is employed. The upper panel shows θ' and u' fields as in Fig. 3 but at a later time, during the statistically steady mature phase. The bottom panel presents the modified PM model storm fields occurring during this same period. The empirically determined w_0 value used was 1.75 m s^{-1}. This value was large enough to have a demonstrable effect without impairing the storm's viability. Increasing w_0 effectively

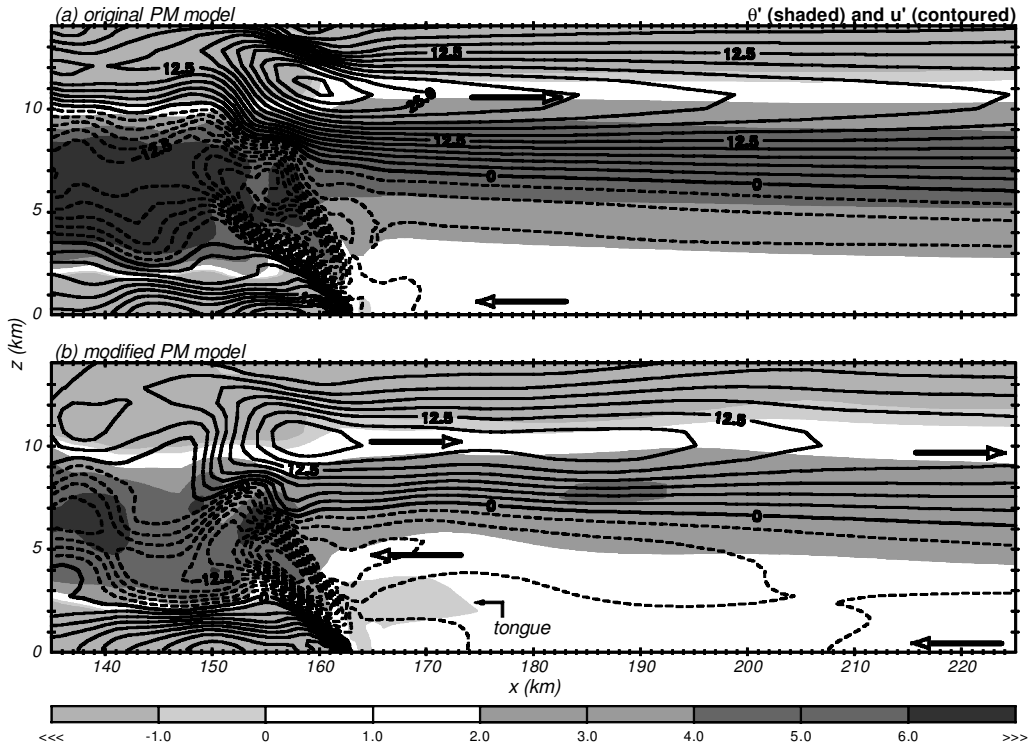

Figure 13. Fields of perturbation horizontal velocity (u', 2.5 m s^{-1} contours) and perturbation potential temperature (θ', shaded) for two parametrized-moisture (PM) model simulations using Fovell and Tan's (2000) moderate convective available potential energy (CAPE) sounding. (a) Original PM model, with updraught threshold $w_0 = 0$. (b) Modified PM model, with $w_0 = 1.75$ m s^{-1}.

renders some fraction of the convective instability inaccessible to the storm. We were unable to find a threshold value that permitted the much more fragile low-CAPE environment to continue supporting deep convection.

Note the modified PM model simulation sports a shallow tongue of chilled air, in roughly the expected position. This localized cooling has resulted in an elevation of the enhanced inflow and a generally more realistic simulation overall, a conclusion also supported by the vertical u_{grnd} profiles of Fig. 14. There are some differences between these two PM simulations. Raising the triggering threshold reduces the total amount of tropospheric warming in the domain, both within and surrounding the convective updraught. With less heating aloft, the cold-pool cooling parameter (θ'_{c}) had to be reduced to obtain roughly the same storm speed of $\approx$15 m s^{-1}. These differences do not appear to invalidate our conclusions.

The present analysis explains why unstable-region truncation had virtually no effect on FT00's simulations. Truncation was intended to prevent parametrized warming in the upstream environment where little if any saturated ascent would be expected. No significant ascent occurred there anyway, at least not in the FT00 cases. In the modified PM framework, however, unstable-region truncation may help the upstream environment to respond properly to elevated cooling near the convection.

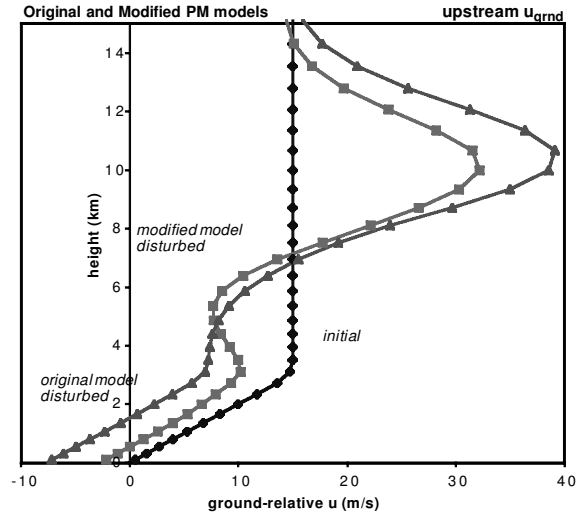

Figure 14. As in Fig. 4 but for the modified parametrized-moisture simulation shown in Fig. 13(b), for comparison with Fig. 10.

5. Discussion and conclusions

The impact of organized convection on its upstream environment was examined using a traditional cloud model as well as a dramatically simplified PM model due to GT and FT00. The study was originally undertaken to explain the differences in mature-phase upstream inflow characteristics noted by FT00.

In both dynamical frameworks, the initial burst of convective heating excited a pair of rapidly propagating gravity waves that were characterized by deep tropospheric subsidence and left the environment surrounding the convection positively buoyant. In the wake of the upstream wave, enhanced flow towards (away from) the convection in the lower (upper) troposphere was noted. The lower-tropospheric inflow was intensified by a non-negligible amount. In the explicit-moisture model, this increased the rate at which moist air from the upstream environment was being fed into the storm, at least during the organizational period.

The model storms in both frameworks eventually settled into extended mature phases possessing upshear-tilted main updraughts modulated by multicellular behaviour. In the more sophisticated model, however, the onset of maturity coincided with the development of a second and markedly different alteration of the storm's upstream environment. This was also attributed to a propagating gravity wave, this time excited by a shallow, weak and yet persistent layer of *mid-tropospheric cooling* which appeared on the upstream side of the main storm updraught around this time.

This secondary wave propagated through the initial wave's wake, substantially altering the upstream environment yet again. It was characterized by lower-tropospheric ascent which served to cool and moisten part of the storm inflow, forming the 'cool/moist tongue'. Importantly, the second wave also caused the upstream inflow enhancement to shift from the surface to the middle troposphere. Although ubiquitous in two- and three-dimensional squall-line simulations made with full-physics cloud models, this second gravity-wave adjustment was completely missing from the original PM model runs.

Analysis suggested that two processes contribute to the establishment and maintenance of the cool/moist tongue: adiabatic expansion of rising subsaturated air and evaporation of cloud droplets detrained from the storm updraught. Neither of these processes were captured in the PM models of FT00 and GT, the former having been absent since all ascent in the unstable region was presumed already saturated. Introducing a minimum updraught speed for parametrized warming generation resulted in a similar tongue-like feature appearing in the PM model simulations as well. With this crude fix, the PM model storms possessed much more realistic upstream structures during the mature phase.

The magnitude of the cooling in the mid-tropospheric tongue is not large, especially when compared with the positive and negative temperature perturbations associated with the convective updraught and sub-cloud cold pool. Its impact on the storm inflow is impressive nonetheless. The cool/moist tongue's associated upstream horizontal velocity perturbations affect the mid-level vertical wind shear in contact with the cold pool and (in the full-physics model) encourages the entrainment of dry, stable mid-tropospheric air into the main storm updraught. Simultaneously, the tongue cooling and moistening established by the gravity-wave response helps bring air above the mixed layer closer to saturation. The 'daughter clouds' that can appear in this elevated layer were found by Fovell and Tan (1998) to play a role in triggering new cell development.

ACKNOWLEDGEMENTS

The author is grateful for discussions with Drs Richard Rotunno, Brian Mapes, Steve Garner, Dave Raymond, Bjorn Stevens and an anonymous reviewer.

REFERENCES

Bretherton, C. S. and Smolarkiewicz, P. K. 1989 Gravity waves, compensating subsidence, and detrainment around cumulus clouds. *J. Atmos. Sci.*, **46,** 740–759

Fovell, R. G. and Ogura, Y. 1988 Numerical simulation of a midlatitude squall line in two dimensions. *J. Atmos. Sci.*, **45,** 3846–3879

1989 Effect of vertical wind shear on numerically simulated multicell storm structure. *J. Atmos. Sci.*, **46,** 3144–3176

Fovell, R. G. and Tan, P.-H. 1998 The temporal behaviour of numerically simulated multicell-type storms. Part II: The convective cell life cycle and cell regeneration. *Mon. Weather Rev.*, **126,** 551–577

2000 A simplified squall-line model revisited. *Q. J. R. Meteorol. Soc.*, **126,** 173–188

Garner, S. T. and Thorpe, A. J. 1992 The development of organized convection in a simplified squall-line model. *Q. J. R. Meteorol. Soc.*, **118,** 101–124

Hoxit, L. R., Chappell, C. F. and Fritsch, J. M. 1976 Formation of mesolows or pressure troughs in advance of cumulonimbus clouds. *Mon. Weather Rev.*, **104,** 1419–1428

Lafore, J.-P. and Moncrieff, M. W. 1989 A numerical investigation of the organization and interaction of the convective and stratiform regions of tropical squall lines. *J. Atmos. Sci.*, **46,** 521–544

Lin, Y.-L. and Smith, R. B. 1986 Transient dynamics of airflow near a local heat source. *J. Atmos. Sci.*, **43,** 40–49

Mapes, B. E. 1993 Gregarious tropical convection. *J. Atmos. Sci.*, **50,** 2026–2037

Nachamkin, J. E. and Cotton, W. R. 2000 Interactions between a developing mesoscale convective system and its environment. Part II: Numerical simulation. *Mon. Weather Rev.*, **128,** 1225–1244

Nicholls, M. E., Pielke, R. A. and Cotton, W. R. 1991 Thermally forced gravity waves in an atmosphere at rest. *J. Atmos. Sci.*, **48,** 1869–1884

Pandya, R. E. and Durran, D. R. 1996 The influence of convectively generated thermal forcing on the mesoscale circulation around squall lines. *J. Atmos. Sci.*, **53,** 2924–2951

Schmidt, J. M. and Cotton, W. R. 1990 Interactions between upper and lower tropospheric gravity waves on squall line structure and maintenance. *J. Atmos. Sci.*, **47,** 1205–1222

Xue, M., Droegemeier, K. K. and Wong, V. 2000 The Advanced Regional Prediction System (ARPS)—a multi-scale nonhydrostatic atmospheric simulation and prediction model. Part I: Model dynamics and verification. *Meteorol. Atmos. Phys.*, **75,** 161–193